Experimental approach to evaluate the influence of characteristic length on the dynamics of biphasic flow in vacuum impregnation

Bruno A.M. Carciofi [a,*], Jhony T. Teleken [a], Vinicius Z. Bertelli [a], Marc Prat [b], João B. Laurindo [a]

[a] Federal University of Santa Catarina, Department of Chemical and Food Engineering, PO BOX 476, 88040-900 Florianópolis, SC, Brazil
[b] Institut de Mecanique des Fluides de Toulouse—Av. Du Professeur Camile Soula, Toulouse, France

HIGHLIGHTS

- The experimental device is a useful tool to investigate the dynamics of vacuum impregnation in porous media.
- Online evolution of the volumetric fraction impregnated at real time.
- We validate the device by comparing with offline balance and with the model for equilibrium.
- Dynamic impregnation is highly affected by the characteristic length, apart from viscosity.

Keywords:
Pore impregnation
Porous media
Food impregnation
Imbibitions
Viscosity
Permeability

ABSTRACT

Vacuum impregnation (VI) is a process of fluid replacement in porous media by reduction in atmospheric pressure and its subsequent reestablishment. The objective of this study was to evaluate the influence of the characteristic length and viscosity of impregnating fluids on vacuum impregnation dynamics. Refractory ceramic samples were used as a non-deformable porous media model, and a device continuously recorded the changes in net force (difference between weight force and buoyant force) on the sample through a load cell during the impregnation process. The relative values for the sample's volumetric fraction due to spontaneous imbibition, for the drained fraction due to vacuum application, and for impregnation due to pressure reestablishment were estimated. The total volumetric fraction estimated during VI by the experimental device was compared with the values estimated by a balance and with those predicted by an equilibrium model. The experimental device was shown to be useful to determine impregnation kinetics, it was accurate and obtained values very close to the ones estimated by the balance and predicted by theoretical models. As expected, the kinetics was dependent on fluid viscosity and on the sample's characteristic length. The kinetics data allowed the minimum time step at the VI process to be determined, enabling the optimization of the process applied to large media or in viscous fluid impregnation.

1. Introduction

Many industrial and natural processes are multiphase fluid flows into porous media such as in oil extraction, textile and food processing, pharmaceutical industries, ceramics and building materials, energy generation, and environmental phenomena. These processes have been widely studied according to various experimental and numerical approaches (Bejan, 1995; Laurindo and Prat, 1996, 1998; Carciofi et al., 2011, 2012; Cai et al., 2012, 2014; Hannach et al., 2014, among others).

Vacuum impregnation (VI) is a hydrodynamic method applied to quickly change the porous medium composition, which, consequently, intensifies the mass transfer in processes in which solid–fluid operations are present by modifying the physical conditions that control this transfer phenomenon. VI occurs in two main steps: (1) vacuum step: Reduction of the chamber pressure where a porous solid is immersed in a liquid; and (2) impregnation step: Atmospheric pressure is reestablished and the impregnating fluid penetrates the porous medium as a result of the global pressure differences (Fito, 1994; Laurindo et al., 2007).

This method enables introducing dissolved or dispersed substances directly into the core of a solid porous structure, increasing the mass transfer rate by reaching shorter diffusive paths after the impregnation step. It can be a tool to prepare supported catalysts,

* Corresponding author. Tel.: +55 48 3721 6408.
E-mail address: bruno.carciofi@ufsc.br (B.A.M. Carciofi).

http://dx.doi.org/10.1016/j.ces.2015.07.052

reinforce materials and structures, and act in osmotic processes and in food impregnation. The literature reports many examples of VI applications: incorporating preservatives or additives into wood and polymers, quickly changing fruit and meat composition, improving oil extraction by liquid solvents, creating new material properties and morphology, accelerating osmotic dehydration, among others (Andrés, 1995; Martínez-Monzó et al., 1998; Chiralt et al., 2001; Betoret et al., 2003; Mújica-Paz et al., 2003a, 2003b; Laurindo et al., 2007; Paes et al., 2007, 2008; Schmidt et al., 2008; Carciofi et al., 2012; Khosrojerdi and Mortazavi, 2013; He et al., 2013; Yang and Qi, 2013; Panarese et al., 2013; Erihemu et al., 2014).

In the first step of VI, the porous medium is exposed to sub-atmospheric pressure for a period of time sufficient to ensure that the fluid flows out of the medium until the internal pressure equalizes the external pressure and some of the liquid trapped in the porous space can be removed. Subsequently, capillary forces promote the natural imbibition of the impregnating liquid into the pore space. In the second step, the atmospheric pressure is reestablished and the external liquid flows into the solid matrix pores as result of the macroscopic pressure gradient, compressing the residual gas until equilibrium is reached (Fito et al., 1996; Laurindo et al., 2007).

The fluid transport properties (viscosity, density), the capillary forces (pore size, surface/interfacial tension, wetting), the porous media characteristics (porosity, tortuosity, polarity, pore distribution, pore network), and the pressure gradients are important parameters to determine the VI dynamics. Furthermore, the macroscopic behavior of fluid intrusion depends on the characteristic length of porous media, i.e., the farthest distance from the surface to a closed region or to a symmetric point.

Fito (1994), Fito and Pastor (1994), and Fito et al. (1996) proposed a mathematical model for VI processes in porous food. It was called hydrodynamic mechanism (HDM) coupled with the deformation–relaxation phenomena (DRP). In the HDM model, VI was modeled as dependent on the food's effective porosity (ε_{ef}, defined as the fraction of the food's total volume occupied by gas) and on the compression rate (r, defined as the ratio between the sum of atmospheric and capillary pressures and the pressure applied during the vacuum step). The HDM model allows evaluating the sample's volumetric fraction impregnated by the external solution due to macroscopic gradients of pressure and the action of capillary forces.

The deformation–relaxation phenomenon (DRP) takes into account the deformations of the porous food in both VI steps by considering the food matrix as a viscoelastic material. Hence, the volumetric fraction of a sample filled with the external solution (X_L) can be estimated by the coupled HDM–DRP model (Eq. (1)). However, the relative sample deformation at the end of the first step (γ_1), and the irreversible relative sample deformation (γ) observed after the second step are required.

$$X_L = \varepsilon_{ef}\left(1-\frac{1}{r}\right)+\gamma \tag{1}$$

The HDM-DRP model is suitable to describe the final state (equilibrium) and can be useful to estimate ε_{ef}. Nevertheless, VI kinetics cannot be described by this model, which does not take into account any transport properties. Carciofi et al. (2011) proposed a two-dimensional mathematical model based on the VOF (Volume of Fluid) model to represent X_L time dependence. Carciofi et al. (2012) extended the model to three-dimensional cases and it was compared to experimental VI data of apples.

Despite all these efforts, some macroscopic properties of fluid-porous medium systems are not included in the previous approaches. Thus, the goal of the present study was to propose an experimental approach in order to evaluate the influence of both characteristic length of a model porous medium and the impregnating fluid's viscosity on the vacuum impregnation dynamics. All VI dynamics data were measured experimentally by a dedicated, purpose-built device. Moreover, these data were compared with the HDM model prediction and with data obtained from a weighing balance.

2. Materials and methods

2.1. Porous media samples

A refractory ceramic block was chosen as a model porous medium. It was cut into parallelepipeds using a diamond saw (Buehler, Isomet 650, USA). In order to evaluate the influence of the sample's characteristic length on VI processes, some surfaces of some samples were sealed using a thin epoxy resin layer (Brascola, Araldite, Brazil), as sketched in Fig. 1. Sixteen samples, identified from A to Q, were used, whose size, mass, and impermeable surfaces are presented in Table 1. The sample sizes (L_x, L_y, and L_z) were determined using a caliper (Mitutoyo Sul Americana, Calibre Model, Brazil) and the dry mass (M_s) was determined using an analytical balance (Shimadzu, AY220, Philippines). All determinations were performed in triplicate, and the average values are presented in Table 1. Sample volume (V_a) was calculated by Eq. (2) and apparent density (ρ_a) was obtained from the M_s/V_a ratio.

$$V_a = L_x L_y L_z \tag{2}$$

Mercury porosimetry (Micromeritics, Poresizer 9320 v2.05, USA) was used to characterize the porous medium regarding the distribution of pore sizes, surface area, and porosity. During intrusion, the working pressure ranged from 0.0012 MPa to 201.1035 MPa. The retraction pressure applied ranged from 141.2017 MPa to 0.0992 MPa. This operating range led to pore sizes from 1000 to 0.0062 μm. In order to obtain the cumulative

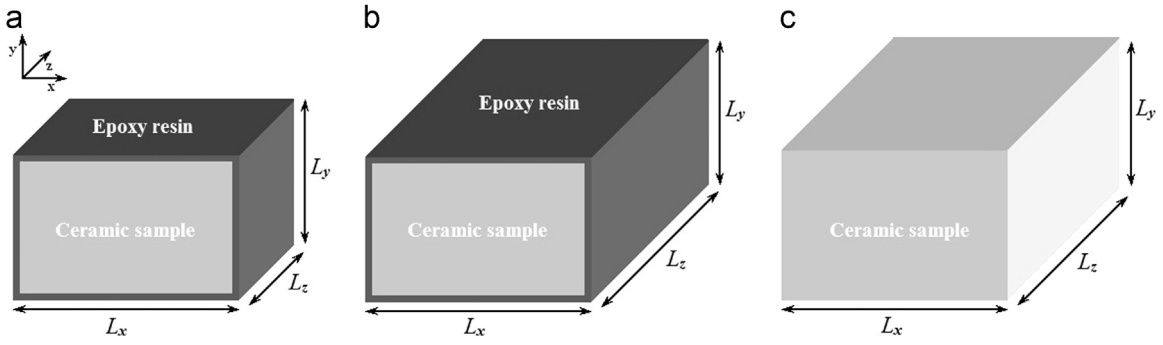

Fig. 1. Sketch of the ceramic samples: (a) sample A with 5 impermeable faces and characteristic length close to 3 cm, (b) sample O with 5 impermeable faces and characteristic length close to 7.5 cm, (c) sample Q with all faces open (no impermeable surfaces).

Table 1
Ceramic samples' characteristics.

Sample code	Edges (10^{-2} m)			M_s (10^{-3} kg)	V_a (10^{-6} m^3)	ρ_a (10^3 kg m^{-3})	Impermeable faces perpendicular to the axis		
	L_x	L_y	L_z				x	y	z
A	3.15	2.93	7.31	129.3526	67.5	1.92	2	2	1
B	3.19	2.88	7.35	128.3090	67.5	1.90	2	2	0
C	3.09	2.87	7.50	126.4586	66.5	1.90	1	2	0
D	3.07	3.10	7.34	133.8790	69.9	1.92	1	1	0
E	3.10	3.05	7.89	133.9746	74.6	1.80	1	0	0
F	2.76	3.07	7.86	120.9848	66.6	1.82	0	0	0
G	3.12	2.74	3.02	46.9465	25.8	1.82	0	0	0
H	3.16	2.96	2.94	50.5281	27.5	1.84	0	0	0
I	3.24	3.11	2.97	56.0339	29.9	1.87	0	0	0
J	3.02	3.03	3.06	50.5780	28.0	1.81	1	0	0
L	3.11	3.38	3.07	56.0576	32.3	1.74	1	1	0
M	3.28	3.05	3.00	51.5280	30.0	1.72	1	1	1
N	3.29	3.18	3.02	55.4428	31.6	1.75	2	2	0
O	3.28	3.23	3.05	56.0250	32.3	1.73	2	2	1
P	3.22	2.85	3.13	51.1940	28.7	1.78	2	2	1
Q	3.00	2.75	8.92	139.1803	73.6	1.89	0	0	0

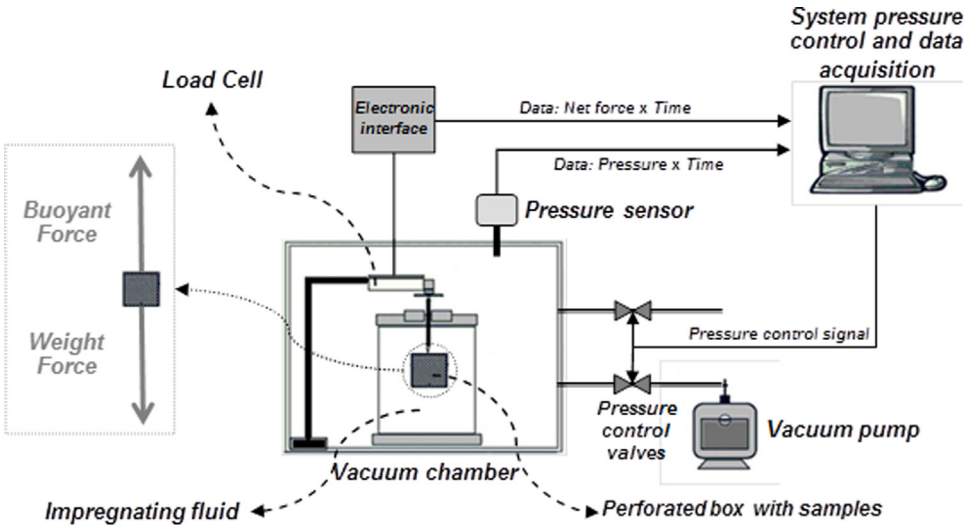

Fig. 2. Schematics of the experimental device used to investigate the vacuum impregnation process kinetics, showing details of the forces acting on the system formed by the rigid rod and the perforated box containing the samples (adapted from Carciofi et al. (2012)).

distribution of pore volume as a function of pore radii (R_c), Laplace's equation (Eq. (3)) was used.

$$P_c = \frac{2\sigma \cos\theta}{R_c} \tag{3}$$

in which P_c is the capillary pressure to be reached, σ is the surface tension of the impregnating fluid, and θ is the contact angle of the mercury over the solid matrix, inside the pore. It can be considered that $\sigma = 0.48$ N m^{-1} and $\theta = 2.44$ rad (Merouani, 1987 apud Mendes, 1997).

2.2. Experimental setup

Sample mass as a time function during the degasification and impregnation steps was measured by a device specially built for this end. It was based on the apparatus proposed by Fito et al. (1996) and by Laurindo et al. (2007). A schematic representation of this device is shown in Fig. 2. It consists of a 50 L vacuum chamber, a vacuum pump (VEB, Model AD230, Germany), and a digital vacuum meter (Motorola, Freescale Semiconductor—MPX2102AP, EUA) for online pressure monitoring. Inside the chamber, a single-point load cell (Alfa Instrumentos, Model GL1, Brazil) with nominal capacity of 1 kg and readability of 0.1 g was sustained by a metallic support. A perforated stainless steel cylindrical box was connected to the load cell by a rigid rod with threaded ends. This system was placed into the vacuum chamber to maintain the sample immersed in the solution. An electronic interface (Alfa Instrumentos, Model 3102, Brazil) connected the load cell to a computer, allowing the net force variations during the experiments to be recorded online. The force measured by the load cell is the net force, which depends on the mass (weight force) and volume (buoyant force) variations of the system (Fig. 2). The device recorded the changes in net force (F_{net}) over time during the whole vacuum impregnation process, as shown in Eq. (4).

$$\frac{F_{net}}{g} = (M_a + M_h) - \rho_L (V_a + V_h) \tag{4}$$

in which g is the acceleration due to gravity, ρ_L is the density of the impregnating solution, M_a is the mass of the sample at a given instant, M_h is the mass of the rigid rod and perforated box, V_a is the volume of the sample at a given moment, and V_h is the volume of the rigid rod and perforated box immersed in the impregnating solution.

The density of the impregnating solution, along with the mass and the volume of the metallic container, are assumed as constant

during the VI process. Hence, the changes in net force during the VI process are due to changes in sample volume, as a consequence of deformation–relaxation phenomena, and in sample mass due to the external solution penetration or native solution drainage. Both V_a and M_a are time-dependent variables. In the VI process, volumetric expansions and native solution loss during vacuum application decrease the net force. On the other hand, both sample impregnation and possible sample shrinking after the atmospheric pressure reestablishment increase the sample's weight. However, in this study, the refractory ceramic sample does not deform under vacuum conditions, thus the resulting force evolution measured by the load cell directly represents the sample's mass loss (degasification step) or mass gain (impregnation step). In this case, the only time-dependent variable (Eq. (4)) is the sample's mass, M_a.

The experimental device also allows controlling the vacuum curves, i.e., the evacuation rate (first step) and the rate of atmospheric pressure recovery (second step), by means of two solenoid valves (Ascoval, model TLP 584127, Brazil). One valve was installed in the suction line, between the vacuum pump and the vacuum chamber (on-off operation) and the other, operating by pulse-width modulation (PWM), was used to allow air to enter the vacuum chamber to help control the pressure.

2.3. Vacuum impregnation experiments

Distilled water was used as the impregnating fluid for samples A to P and analytical grade glycerol was used for samples F to I and Q, both fluids kept at 25 °C. The physical properties (density, ρ_L, dynamic viscosity, μ, and surface tension, σ) of both fluids are given in Table 2. The choice of fluids aimed to investigate the influence of their viscosities on the dynamics of VI processes, because, at 25 °C, glycerol viscosity is about 1000 times higher than water viscosity. Prior to vacuum impregnation experiments, previously dried samples were submitted to spontaneous imbibition by submerging them in a vessel with the impregnating solution for 24 h.

For the vacuum impregnation process, the ceramic samples were placed in the perforated stainless steel cylindrical box and submerged into the impregnating liquid inside the vacuum chamber, initially at atmospheric pressure (Fig. 2). Vacuum pressure (P_1=46.7 kPa) was applied for 240 s (45 s for reducing the pressure from P_{atm} to P_1, i.e., reduction of approximately 54% of P_{atm}), and 420 s for reestablishing atmospheric pressure (P_2), which characterized one VI cycle. Each sample was subjected to ten VI cycles. Aiming to correct the effects of vacuum on the load cell, some tests were performed with the perforated cylinder without samples, submerged in the impregnating solution.

2.4. Experimental determination of mass exchanges

The weights of the ceramic samples were determined with a semi-analytical balance (Tecnal Line 6k, Brazil), before (M_{a0}) and after (M_{a2}) each vacuum impregnation experiment, as well as the mass of dry samples (M_{aS}), i.e., before the spontaneous imbibition. The relative mass gain during vacuum impregnation (GB) (Eq. (5)) and the relative mass gain due to spontaneous imbibition (GB_{eb}) (Eq. (6)) were both determined in relation to M_{aS}. The relative total weight gain (GB_T) was determined by summing GB and GB_{eb} (Eq. (7)).

Table 2
Physical properties of distilled water and glycerol at 25 °C (Lide, 2004).

Fluid	ρ_L (kg m^{-3})	μ (mPa s)	σ (mN m^{-1})
Water	997.05	0.890	72.0
Glycerol	1257.8	934.0	62.5

$$GB = \frac{M_{a2} - M_{a0}}{M_{aS}} \tag{5}$$

$$GB_{eb} = \frac{M_{a0} - M_{aS}}{M_{aS}} \tag{6}$$

$$GB_T = \frac{M_{a2} - M_{aS}}{M_{aS}} \tag{7}$$

The relative gain of total weight (in relation to initial mass, M_{a0}) during the vacuum impregnation (GC) process was calculated from the values recorded by the load cell at the beginning (F_{net0}/g) and at the end of the process (F_{net2}/g), as given by Eq. (8). The mass gains in step 1 (vacuum step—GC_1) and in step 2 (impregnation step—GC_2) were determined by the load cell, and the relative mass gains were calculated with Eqs. (9) and (10), respectively.

$$GC = \frac{F_{net2} - F_{net0}}{gM_{a0}} \tag{8}$$

$$GC_1 = \frac{F_{net1} - F_{net0}}{gM_{a0}} \tag{9}$$

$$GC_2 = \frac{F_{net2} - F_{net1}}{gM_{a0}} \tag{10}$$

The mass of fluid drained from the sample during the first stage (M_d), due to the expansion of the gases contained in the porous space, was defined by Eq. (11).

$$M_d = M_{a0} - M_{a1} \tag{11}$$

where M_{a1} is the sample weight at the end of step 1.

The value GC_1 is proportional to the drained mass as a result of vacuum application in step 1. Thus, for a non-deformable sample, the mass of fluid drained during vacuum application was estimated by Eq. (12), while the volumetric fraction of liquid drained due to vacuum application (X_D) was calculated by Eq. (13).

$$M_d = GC_1 M_{a0} \tag{12}$$

$$X_D = \frac{M_d}{V_a \rho_L} \tag{13}$$

The volumetric fraction of the sample impregnated as a result of spontaneous imbibition was determined by Eq. (14).

$$X_{Leb} = \frac{GB_{eb} M_{aS}}{V_a \rho_L} \tag{14}$$

From the value of X_{Leb}, a representative value of P_c could be estimated by Eq. (15). The estimated value of P_c is a way of representing the matric potential of the porous medium.

$$P_c = \frac{X_{Leb}}{(\varepsilon_e - X_{Leb})} P_2 \tag{15}$$

The volumetric fraction of the sample impregnated at the end of the whole process (X_L^B), as determined by experimental data measured by the balance, is given by Eq. (16).

$$X_L^B = \frac{GB_T M_{aS}}{V_a \rho_L} \tag{16}$$

From the dynamic values registered by the load cell, the fraction of the sample impregnated in step 2 (X_{L2}^C), which is promoted by the overall gradients of pressure created by the reestablishment of atmospheric pressure, is given by Eq. (17).

$$X_{L2}^C = \frac{GC_2 M_{a0}}{V_a \rho_L} \tag{17}$$

The volumetric fraction of the impregnated sample, determined from the load cell data (X_L^C), is calculated with Eq. (18).

$$X_L^C = X_{Leb} + X_D + X_{L2}^C \tag{18}$$

where X_{Leb} is the contribution of the fraction impregnated by spontaneous imbibition, X_D represents the fraction of fluid drained during vacuum application, and X_{L2}^C is the fraction impregnated during the second step of the VI process.

In this study, the VI experiments were performed with the ceramic samples previously submitted to spontaneous imbibition. Thus, the effective porosity could be corrected by discounting the volume of air replaced by the liquid and defining a corrected effective porosity, ε_e^*, given by Eq. (19). Thus, X_L^* is the volumetric fraction calculated using ε_e^*, neglecting the value of P_c. The effects of P_c were considered by discounting the volume filled during spontaneous imbibition (as a result of the porous medium matric potential) from ε_e. Therefore, the equilibrium situation, adapted from the HDM, is given by Eq. (20).

$$\varepsilon_e^* = \varepsilon_e - X_{Leb} \tag{19}$$

$$X_L^* = \varepsilon_e^* \left(1 - \frac{P_1}{P_2}\right) \tag{20}$$

3. Results and discussion

The pore size distribution in the samples from mercury porosimetry analyses is shown in Fig. 3. Hysteresis phenomenon between intrusion and extrusion was observed, mainly for pore diameters greater than 0.100 μm. This difference is explained by the presence of narrows at the entrance of large pores, where mercury penetration depends on the narrow's radius, as given by Laplace's equation. For pore sizes of approximately 10.000 μm, the volume of mercury in the sample during extrusion was twice the volume accumulated during intrusion. These results indicate that the ceramic sample has most of its volume formed by pores with diameters greater than 10.000 μm and that about half of this volume is related to pores with a constriction. The estimated porosity was 0.244.

Representative experimental results of ceramic pieces (sample H) subjected to VI process are shown in Fig. 4. It presents the resultant force (measured by the load cell) on the perforated cylinder containing the sample and the total pressure inside the vacuum chamber.

The mass changes of the samples during VI experiments are presented in Tables 3 and 4. The average values and the variation coefficient (VC [%] = 100 × standard deviation/mean value) of X_{Leb}, P_c, X_D, X_{L2}^C, X_L^C, and X_L^B were calculated from ten repetitions, while the values of X_L (Eq. (1)) and X_L^* (Eq. (20)) were estimated by the HDM. The values of X_L were calculated with values of P_1 and P_2 determined experimentally, average values of P_c were estimated (Eq. (15)) for each sample-impregnating solution set, while the effective porosity of the dry sample was determined by mercury intrusion (ε_e = 0.244). Data presented in Tables 3 and 4 were analyzed by Tukey's test using a 95% confidence level.

The values of X_{Leb}, P_c, X_D, and X_{L2}^C showed no relationship with the number of open and closed sides, or with the sample size. The VC values on X_{Leb} are considered low because only three out of 20 sample-impregnating solution sets had VC above 5% and none was higher than 10%. Although the samples were obtained from a single ceramic block, some of the 20 estimated values of P_c were different, i.e., ten samples had VC values lower than 5%, while for five samples this coefficient was higher than 10%.

As the values of M_d were close to the accuracy of the load cell, the values determined for X_D had high VC values and many of them had no significant differences. It was observed that the highest values of X_D were found for samples with smaller dimensions and fully open (G, H, and I) when soaked in water. Moreover, for these same three samples, X_D was significantly lower for immersion in glycerol than the value obtained for immersion in water. The high viscosity of glycerol (more than 1000 times higher if compared to water) may explain the greater difficulty in drainage. The high viscosity of glycerol may also explain the difference between the values of X_{Leb} found for the same sample immersed in different fluids, because an amount of glycerol greater than water was adhered to sample's surface when the weights were determined.

Despite having very different viscosities, glycerol and water are polar molecules able to form hydrogen bonds, are mutually miscible, and have similar density values (Table 2). Therefore, similar values can be expected for θ of both fluids at the same surface. If the surface tension values are close (Table 2), one could suppose that the values of P_c, and also of X_{Leb}, should be similar for the same sample immersed in either water or glycerol. The contact

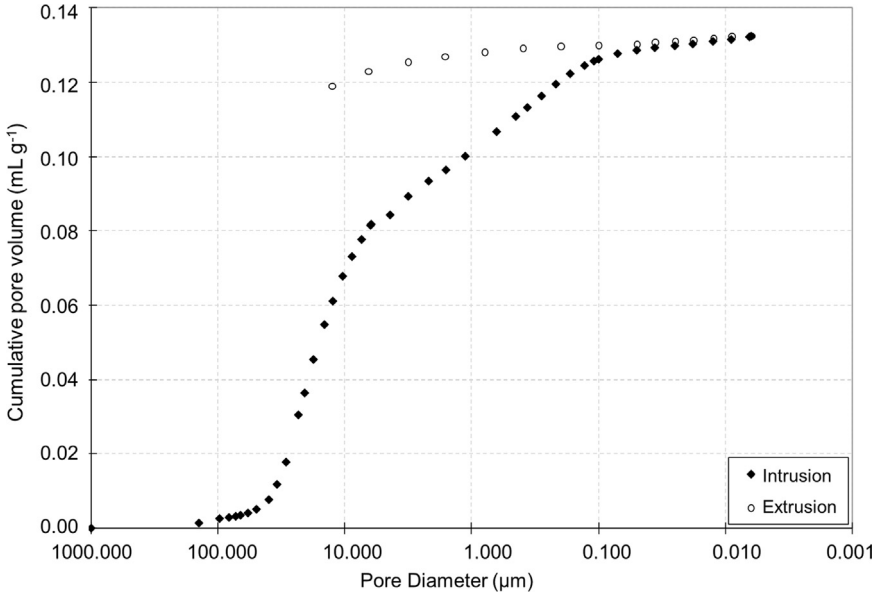

Fig. 3. Mercury porosimetry results of the ceramic samples.

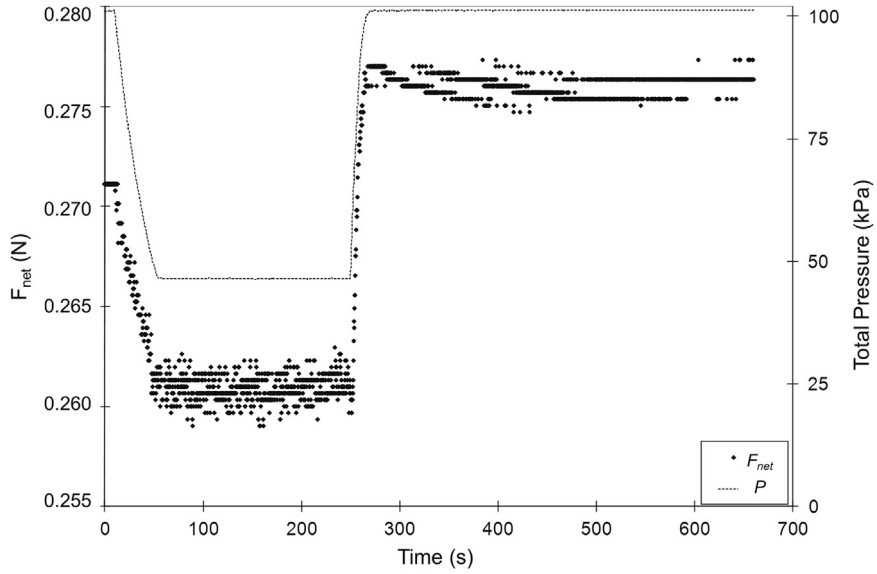

Fig. 4. Time evolution of the resultant force on the system formed by the perforated box and the rigid rod, and of the total pressure inside the vacuum chamber during VI of sample H immersed in water.

Table 3
VI parameters X_{Leb}, P_c, X_D, and X_{L2}^C, average values, and variation coefficients (VC).

Sample	Impregnating fluid	X_{Leb}		P_c (kPa)		X_D		X_{L2}^C	
		Mean	VC (%)	Mean	VC (%)	Mean	VC (%)	Mean	VC (%)
A	Water	0.130^{fg}	2.78	117^{ef}	6.05	0.0248^{cde}	21.0	0.0609^{cd}	6.50
B	Water	0.117^{c}	3.81	95.5^{cd}	7.76	0.0286^{bcd}	17.7	0.0623^{d}	6.46
C	Water	0.153^{m}	0.87	171^{j}	2.20	0.0356^{abc}	10.2	0.0603^{cd}	3.36
D	Water	0.120^{cde}	1.94	100^{cd}	4.38	0.0310^{abcd}	13.4	0.0602^{cd}	5.26
E	Water	0.126^{ef}	1.70	110^{de}	3.73	0.0333^{abcd}	20.4	0.0630^{d}	10.2
F	Water	0.143^{hij}	1.55	146^{gh}	4.48	0.0297^{bcd}	40.9	0.0534^{abc}	22.0
F	Glycerol	0.148^{ijl}	3.88	158^{hij}	10.5	0.0204^{de}	25.8	0.0491^{a}	12.2
G	Water	0.136^{gh}	1.80	130^{fg}	4.25	0.0412^{ab}	32.7	0.0389^{abc}	19.8
G	Glycerol	0.146^{ijl}	4.07	153^{ghi}	10.6	0.0181^{de}	35.4	0.0502^{ab}	13.7
H	Water	0.105^{b}	5.55	77.2^{ab}	8.95	0.0455^{a}	18.9	0.0575^{abc}	14.4
H	Glycerol	0.160^{m}	4.19	195	12.1	0.0243^{cde}	35.7	0.0364^{abcd}	12.5
I	Water	0.094^{a}	5.46	63.7^{a}	9.60	0.0410^{ab}	41.7	0.0425^{abc}	33.2
I	Glycerol	0.125^{def}	8.31	109^{de}	17.2	0.0198^{de}	35.6	0.0562^{a}	20.5
J	Water	0.141^{hi}	2.57	142^{gh}	6.58	0.0321^{abcd}	36.3	0.0585^{abc}	21.5
L	Water	0.118^{cd}	1.97	95.9^{cd}	3.98	0.0299^{bcd}	34.8	0.0489^{abc}	19.9
M	Water	0.118^{cd}	1.59	96.2^{cd}	2.14	0.0233^{cde}	28.2	0.0552^{abc}	12.8
N	Water	0.103^{b}	2.10	75.8^{ab}	3.39	0.0186^{de}	25.5	0.0389^{abcd}	7.53
O	Water	0.115^{c}	2.24	91.4^{bc}	4.41	0.0146^{e}	33.1	0.0552^{a}	9.29
P	Water	0.119^{cde}	1.95	98.2^{cd}	3.69	0.0209^{cde}	24.2	0.0565^{abc}	6.26
Q	Glycerol	0.150^{jl}	4.88	166^{ij}	13.4	0.0186^{de}	19.4	0.0436^{ab}	3.55

The same lowercase letter in the same column means that there are no significant differences between the values at 95% confidence level by Tukey's test.

angle of glycerol on glass was calculated and determined experimentally by Njobuenwu et al. (2007), who reported values of 28.5° and 24.78°, respectively. These values are of the same order of the value reported by Mohammadi and Amirfazli (2005), 27°. As expected, no significant differences in the values of P_c and X_{Leb} were observed for impregnation with water and glycerol for samples F and G. However, for samples H and I, P_c and X_{Leb} were significantly higher when glycerol was the impregnating fluid.

The values of total volumetric fraction impregnated by the liquid at the end of the VI process are given in Table 4. Parameters X_L^C and X_L^B were significantly different in 14 of 20 sample-impregnating fluid sets, but the percentage difference between these values did not exceed 10% in any of the sets evaluated. All values of X_L estimated by the HDM were outside the confidence interval of the values determined experimentally for all sets. However, the corrected X_L^*, also determined by the HDM, matched at least one of the values (X_L^C or X_L^B) in 15 of the 20 sets evaluated.

Comparing the samples impregnated with water or glycerol, no significant differences were observed between the values of X_L^C for sample F and between the values of X_L^B for samples F and G. The values of X_L^C for samples G, H, and I and the values of X_L^B for samples H and I showed significant differences. Besides, all parameters were higher when glycerol was used as the impregnating fluid. This behavior is directly related to the values obtained for parameters X_D and X_{Leb} (Table 3), which may be due to the high viscosity of glycerol, as previously discussed.

The calculations of X_L^C and X_L^B were reproductive, and the VC values for the former were lower than 5.0% in 18 of 20 sample-impregnating fluid sets, remaining always below 10.0%. The parameter X_L^B showed variation coefficient values lower than 3.0% in 19 of 20 samples, confirming the accuracy of the experimental determinations. Mean temporal evolution values of the samples' impregnated volumetric fraction during the second step of the VI process (X_{L2t}^C) are shown in Fig. 5 for samples with approximate

Table 4
Parameters X_L^C and X_L^B (average values and variation coefficients, VC), X_L estimated by the HDM (Eq. (1)) and X_L^* estimated by Eq. (20).

Sample	Impregnating fluid	X_L^C		X_L^B		X_L	ε_e^*	X_L^*
		Mean	VC (%)	Mean	VC (%)			
A	Water	0.166^{Ad}	1.95	0.167^{Afg}	0.99	0.192^{B}	0.114	0.166^{A}
B	Water	0.151^{Afgh}	2.33	0.156^{Be}	1.48	0.186^{C}	0.127	0.156^{AB}
C	Water	0.177^{Aab}	2.03	0.183^{Bj}	0.71	0.202^{C}	0.091	0.166^{D}
D	Water	0.149^{Afgh}	1.42	0.155^{Be}	1.04	0.187^{C}	0.124	0.155^{B}
E	Water	0.156^{Aef}	2.02	0.163^{Bf}	1.06	0.190^{C}	0.118	0.156^{A}
F	Water	0.167^{Acd}	1.76	0.175^{Bhi}	1.29	0.198^{C}	0.101	0.167^{A}
F	Glycerol	0.166^{Ad}	3.21	0.171^{ABgh}	2.32	0.200^{C}	0.096	0.179^{B}
G	Water	0.152^{Afg}	2.61	0.166^{Bfg}	0.97	0.194^{C}	0.108	0.153^{A}
G	Glycerol	0.168^{Abcd}	4.08	0.167^{ABfg}	2.09	0.199^{C}	0.098	0.180^{B}
H	Water	0.118^{Al}	4.10	0.131^{Bb}	1.47	0.180^{C}	0.139	0.134^{B}
H	Glycerol	0.184^{Aa}	3.64	0.184^{Aj}	0.34	0.205^{B}	0.084	0.180^{A}
I	Water	0.108^{Am}	5.39	0.117^{Ba}	2.17	0.174^{C}	0.150	0.133^{D}
I	Glycerol	0.144^{Aghi}	8.42	0.148^{ABd}	7.36	0.189^{C}	0.119	0.169^{B}
J	Water	0.164^{Ade}	3.02	0.173^{Bh}	1.19	0.197^{C}	0.103	0.164^{A}
L	Water	0.144^{Aghi}	1.94	0.152^{Bde}	1.28	0.186^{C}	0.126	0.155^{B}
M	Water	0.144^{Ahi}	2.06	0.153^{Bde}	0.78	0.186^{C}	0.126	0.162^{D}
N	Water	0.135^{Aj}	2.23	0.141^{Bc}	0.87	0.180^{C}	0.141	0.160^{D}
O	Water	0.136^{Aij}	1.64	0.142^{Bc}	0.97	0.185^{C}	0.129	0.169^{D}
P	Water	0.154^{Af}	2.11	0.162^{Bf}	0.38	0.187^{C}	0.125	0.165^{B}
Q	Glycerol	0.175^{Aabc}	3.73	0.180^{Aij}	2.72	0.201^{B}	0.094	0.182^{A}

The same lowercase letter in the same column and the same uppercase letter in the same row mean that there are no significant differences between the values at 95% confidence level by Tukey's test.

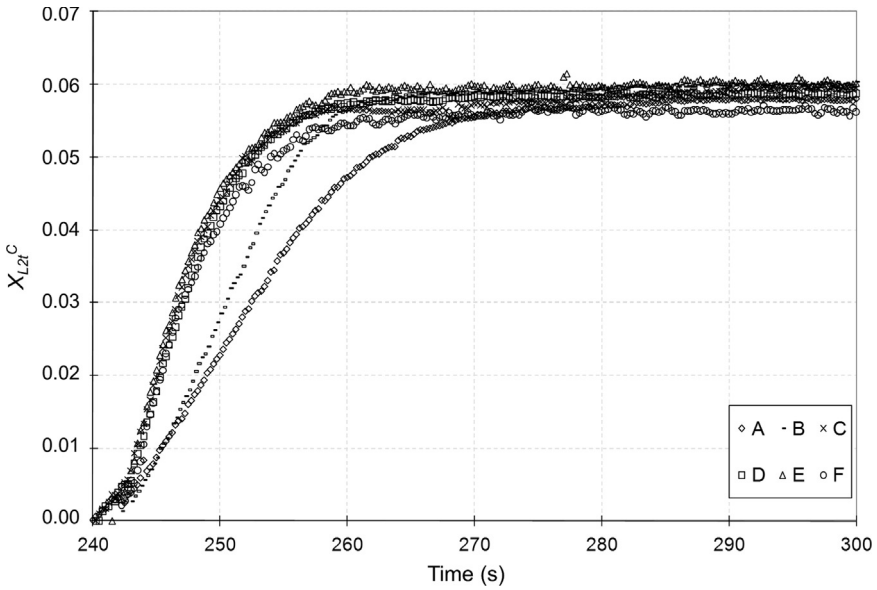

Fig. 5. Time variation of the volumetric fraction of the sample impregnated by liquid during step 2 of the VI process. Comparison of results obtained for samples A, B, C, D, E, and F.

dimensions of $3.0 \times 3.0 \times 7.5$ cm ($L_x \times L_y \times L_z$). It can be observed that the values of X_{Lt}^C for sample A (all faces $L_y \times L_z$ and one face $L_x \times L_y$ are impermeable) showed an inferior slope when compared with the results obtained for sample B (all faces $L_y \times L_z$ are impermeable). For the second sample, the X_{L2t}^C slope decreased when compared with values obtained for samples C, D, E, and F (both smaller faces and one, two, three, or four bigger faces are permeable), which have very similar temporal variations of X_{L2t}^C.

As the samples have approximately the same dimensions, the number of faces covered by the epoxy resin defines the characteristic length for the fluid flow. Samples A and B were impregnated at a slower rate because they have regions in which the shortest length from the surface (characteristic length) is L_z and $L_z/2$ ($L_z \sim 7.5$ cm), respectively, besides the fluid flow in both samples being one-dimensional. Comparing the other four samples, C, D, E, and F, their characteristic lengths are L_x, L_x, $L_x/2$, and $L_x/2$ ($L_x \sim 3.0$ cm), respectively, combined with bi- or three-dimensional fluid flow.

The VI dynamics of the porous samples with water shown in Fig. 6 compares the process for samples A and P. Both have five of the six sides sealed by resin, but the characteristic length for fluid flow is greater for sample A (7.31 cm against 3.13 cm for sample P), leading to a smaller slope of the curve X_{L2t}^C vs. t, i.e., a slower impregnation rate. Fig. 7 presents a comparison of VI dynamics of samples without sealing resin, i.e., with all faces available for the VI process (samples F, G, H, and I). Although sample F has greater dimension than the other samples, the characteristic length for fluid flow is the same for all samples. Moreover, as the fluid flow is three-dimensional, the impregnation rate is about the same for all these samples. These results suggested that, during the impregnation step, the fluid invades samples through preferential ways. If the number of permeable faces increases, pore interconnectivity

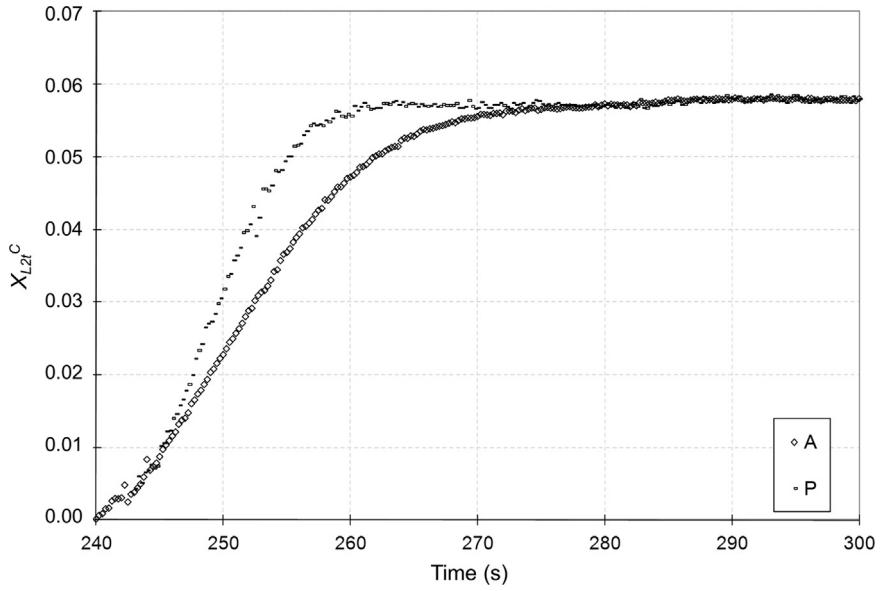

Fig. 6. Time variation of the average volumetric fraction of the sample impregnated by liquid during step 2 of the VI process. Comparison of results obtained for samples A and P.

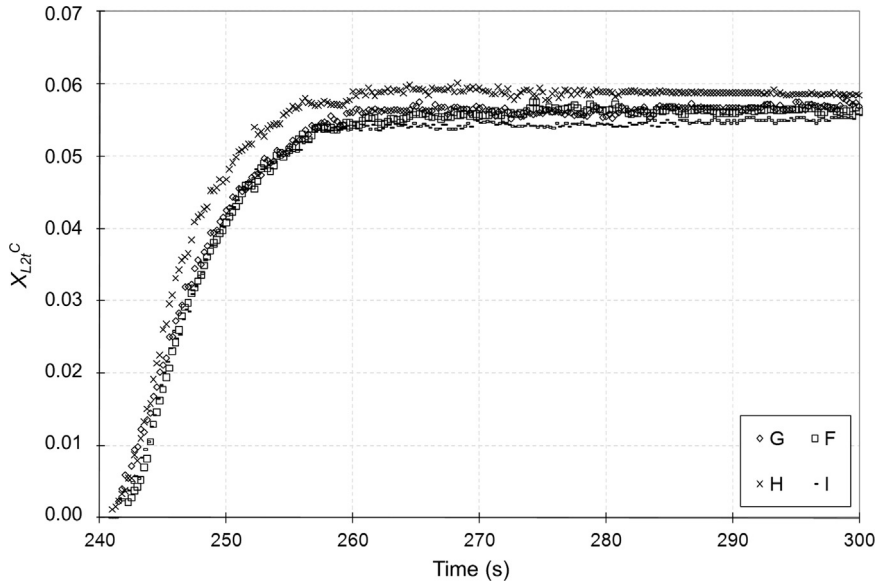

Fig. 7. Time variation of the volumetric fraction of the sample impregnated by liquid during step 2 the of VI process. Comparison of results obtained for samples F, G, H, and I.

also increases, which accelerates the invasion of the impregnating fluid during the impregnation step. This phenomenon has been reported by researchers who investigated the drainage of wetting fluids in porous media by the injection of fluids (Laurindo and Prat, 1996, 1998).

The time for X_{L2t}^{C} to achieve values close to equilibrium for sample A was 50% higher when compared with the results observed for sample P. These results allow evaluating the minimal process time for the VI of larger samples or when high-viscosity fluids are used.

4. Conclusions

The experimental device used to evaluate the VI dynamics of porous media showed to be a useful tool to capture real time sample's changes. Final volumetric fraction of the sample impregnated with liquid determined by the load cell has good accuracy, as proved by the comparison with the offline values determined with the balance. Furthermore, this approach provides the temporal evolution of the volumetric fraction of the sample impregnated and can be used to determine the minimum time of immersion, thus helping the experimental optimization of the VI process with fluids with different viscosities and samples with different characteristic lengths, mainly for irregular or non-classical geometries and highly anisotropic materials.

Glycerol presented the lowest impregnation rate in spite of the slightly higher capillary pressure when compared to water. However, the impregnated volumetric fraction predicted by the model and measured showed significant difference between both fluids for samples with similar characteristic length at the three directions, indicating gas entrapping into the sample. On the other hand, drainage measurement was not accurate enough for the glycerol due to its high viscosity and, consequently, equilibrium values found by load cell can be overestimated for this fluid. In addition, characteristic length showed minor role on the final

impregnated fraction and main role on the dynamics. It is reasonable to expect a pressure gradient on the fluid flowing into the sample, resulting in weaker forces to push and drive out the gas present, which will remain entrapped.

Acknowledgements

The authors thank the Brazilian Council for Scientific and Technological Development (CNPq) and CAPES-Brazil for the financial support.

References

Andrés, A.M., 1995. Impregnación a Vacio en Alimentos Porosos. Aplicación al Salado de Quesos Ph.D Thesis. Universidad Politécnica de Valencia, Espanha.

Bejan, A., 1995. Convective Heat Transfer. John Wiley & Sons, New York, NY.

Betoret, N., Puente, L., Díaz, M.J., Pagán, M.J., García, M.J., Gras, M.L., Martínez-Monzó, J., Fito, P., 2003. Development of probiotic-enriched dried fruits by vaccum impregnation. J. Food Eng. 56, 273–277.

Cai, J., Hu, X., Standnes, D.C., You, L., 2012. An analytical model for spontaneous imbibition in fractal porous media including gravity. Colloids Surf., A: Physicochem. Eng. Aspects 414, 228–233.

Cai, J., Perfect, E., Cheng, C.L., Hu, X., 2014. Generalized modeling of spontaneous imbibition based on Hagen–Poiseuille flow in tortuous capillaries with variably shaped apertures. Langmuir 30 (18), 5142–5151.

Carciofi, B.A.M., Prat, M., Laurindo, J.B., 2011. Homogeneous volume-of-fluid (VOF) model for simulating the imbibition in porous media saturated by gas. Energy Fuels 25, 2267–2273.

Carciofi, B.A.M., Prat, M., Laurindo, J.B., 2012. Dynamics of vacuum impregnation of apples: experimental data and simulation results using a VOF model. J. Food Eng. 113, 337–343.

Chiralt, A., Fito, P., Barat, J.M., Andrés, A., González-Martínez, C., Escriche, I., Camacho, M.M., 2001. Use of vaccum impreganation in food salting process. J. Food Eng. 49, 141–151.

Erihemu, K., Hironaka, K., Oda, Y., Koaze, H., 2014. Iron enrichment of whole potato tuber by vaccum impregnation. LWT—Food Sci. Technol. 59, 504–509.

Fito, P., 1994. Modelling of vaccum osmotic dehydratation of food. J. Food Eng. 22, 313–328.

Fito, P., Pastor, R., 1994. Non-diffusional mechanisms occurring during vacuum osmotic dehydration. J. Food Eng. 21, 513–519.

Fito, P., Andrés, A., Chiralt, A., Pardo, P., 1996. Coupling of hydrodynamic mechanism and deformation—relaxation phenomena during vacuum treatments in solid porous food-liquid systems. J. Food Eng. 27, 229–240.

He, T., Ren, X., Cai, K., Wei, Y., Sun, S., 2013. Electrochemical performance of activated carbon treated by vacuum impregnation using fluorinated surfactant. Mater. Technol. 28, 364–369.

Khosrojerdi, M., Mortazavi, S.M., 2013. Impregnation of a porous material with a PCM on a cotton fabric and the effect of vacuum on thermo-regulating textiles. J. Therm. Anal. Calorim. 114, 1111–1119.

Laurindo, J.B., Prat, M., 1996. Numerical and experimental network study of evaporation in capillary porous media. Phase distributions. Chem. Eng. Sci. 51, 5171–5185.

Laurindo, J.B., Prat, M., 1998. Numerical and experimental network study of evaporation in capillary porous media. Drying rates. Chem. Eng. Sci. 53, 2257–2269.

Laurindo, J.B., Stringari, G.B., Paes, S.S., Carciofi, B.A.M., 2007. Experimental determination of the dynamics of vacuum impregnation of apples. J. Food Sci. 72, E470–E475.

Lide, D.R. (Ed.), 2004. Handbook of chemistry and physics. 84 ed., CRC Press LLC.

Martínez-Monzó, J., Martínez-Navarrete, N., Chiralt, A., Fito, P., 1998. Mechanical properties and structural changes in apple (Var. Granny Smith) due to vacuum impregnation with cryoprotectants. J. Food Sci. 63, 499–503.

Merouani, L., 1987. Phénomènes de sorption et de transfert d'humidité dans des matériaux du bâtiment : étude expérimentale comparative d'un mortier de ciment et d'un enduit de façade Ph.D Thesis. I.N.P.G., Grenoble, France.

Mendes, N., 1997. Modelos para a Previsão de Transferência de Calor e de Umidade em Elementos Porosos de Edificações Ph.D Thesis. Departamento de Engenharia Mecânica, Universidade Federal de Santa Catarina, Florianópolis.

Hannach, M., Soboleva, T., Malek, K., Franco, A.A., Prat, M., Pauchet, J., Holdcroft, S., 2014. Characterization of pore network structure in catalyst layers of polymer electrolyte fuel cells. J. Power Sources 247, 322–326.

Mohammadi, R., Amirfazli, A., 2005. Contact angle measurement for dispersed microspheres using scanning confocal microscopy. J. Dispersion Sci. Technol. 25, 567–574.

Mújica-Paz, H., Valdez-Fragoso, A., López-Malo, A., Palou, E., Welti-Chanes, J., 2003a. Impregnation and osmotic dehydration of some fruits effect of the cacuum pressure and syrup concentration. J. Food Eng. 57, 305–3014.

Mújica-Paz, H., Valdez-Fragoso, A., López-Malo, A., Palou, E., Welti-Chanes, J., 2003b. Impregnation properties of some fruits at vaccum pressure. J. Food Eng. 56, 307–3014.

Njobuenwu, D.O., Oboho, E.S., Gumus, R.H., 2007. Determination of contact angle from contact area of liquid droplet spreading on solid substrate. Leonardo Electron. J. Pract. Technol. 6, 29–38.

Paes, S.S., Stringari, G.B., Laurindo, J.B., 2007. Effect of vacuum and relaxation periods and solutions concentration on the osmotic dehydration of apples. Int. J. Food Sci. Technol. 42, 441–447.

Paes, S.S., Stringari, G.B., Laurindo, J.B., 2008. Effect of vacuum impregnation temperature on the mechanical properties and osmotic dehydration parameters of apples. Braz. Arch. Biol. Technol. 51, 779–806.

Panarese, V., Dejmek, P., Rocculi, P., Galindo, F.G., 2013. Microscopic studies providing insight into the mechanisms of mass transfer in vacuum impregnation. Innovative Food Sci. Emerg. Technol. 18, 169–176.

Schmidt, F.C., Carciofi, B.M.C., Laurindo, J.B., 2008. Efeito da impregnação a vácuo na transferência de massa durante o processo de salga de cortes de peito de frango. Ciência e Tecnologia de Alimentos 28, 366–372.

Yang, L.N., Qi, M.L., 2013. Rapid fabrication of confined Au nanoparticles with tunable sizes and morphologies by a simple glucose-assisted vacuum impregnation method. Mater. Lett. 98, 74–77.